THE JOURNAL OF PHYSICAL CHEMISTRY A
A JOURNAL OF THE AMERICAN CHEMICAL SOCIETY

pubs.acs.org/JPCA

Article

Molecular Structures and Microwave Spectra of the Gas-Phase Homodimers of 3-Fluoro-1,2-epoxypropane and 3,3-Difluoro-1,2-epoxypropane

Published as part of The Journal of Physical Chemistry virtual special issue "Marsha I. Lester Festschrift".

Mark D. Marshall* and Helen O. Leung*

Cite This: https://doi.org/10.1021/acs.jpca.3c03643

Read Online

ACCESS | Metrics & More | Article Recommendations | Supporting Information

ABSTRACT: Molecular structures for the heterochiral and homochiral gas-phase homodimers of 3-fluoro-1,2-epoxypropane and 3,3-difluoro-1,2-epoxypropane are investigated using both ab initio and density functional quantum chemistry calculations. Although microwave spectra for the heterochiral dimers are not observed as the lowest-energy isomers lack an electric dipole moment and others are presumably too high in energy, rotational spectra are observed for the homochiral dimers of each molecule that are consistent with the lowest-energy isomers of each. The presence of hydrogen atoms in the fluoromethyl groups makes it possible for these groups to participate in the intermolecular interactions that stabilize these dimers, resulting in a distinctly different bonding motif than is observed in the homodimers of 3,3,3-trifluoro-1,2-epoxypropane where the lack of a hydrogen atom prevents this possibility. The rotational spectra and energy ordering of the dimers are sufficiently well predicted with modest calculational methods to enable straightforward assignment of the observed spectra and to identify the molecular carrier of an assigned spectrum.

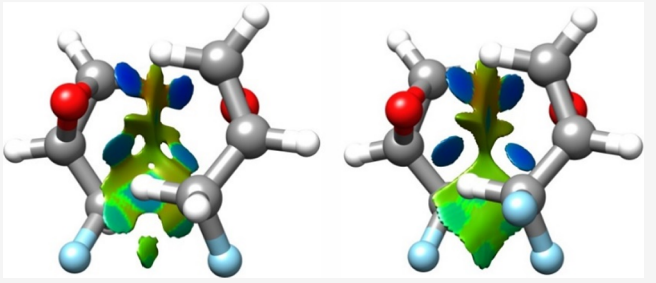

1. INTRODUCTION

Our search for effective chiral tags has revealed that epoxides substituted with fluorine atoms are good candidates. Thus far, we have studied and reported the rotational spectra of three epoxides with a fluoromethyl group ($-CH_nF_{3-n}$, where $n = 0-2$).[1−3] These epoxides have several desirable attributes. The relative ease of introduction of these species into free jet expansion and the existence of multiple functional groups suggest that they should be able to establish favorable intermolecular interactions with a pair of enantiomeric analytes so that the use of an enantiopure form of the tag would convert the enantiomers into spectroscopically distinct diastereomeric dimers, thus allowing the identification of the absolute configurations of the analytes and the determination of their relative amounts in the original sample.[4−10] Because each of these epoxides has relatively small moments of inertia, the rotational constants for the diastereomeric dimers are reasonably large, which, together with the absence of hyperfine interactions and internal dynamics in the epoxide, results in little spectral congestion or complication in analyzing the dimeric spectra.

We have shown in two experiments that indeed, 3,3,3-trifluoro-1,2-epoxypropane [2-(trifluoromethyl)oxirane or TFO] works well as a chiral tag. In a collaboration with the Schnell group, an enantiopure sample of TFO, (*R*)-TFO, is used for chiral analysis.[7] By complexing this tag with a sample containing a mixture of styrene oxide (SO) enantiomers, we unambiguously identify and distinguish the two complexes, (*R*)-TFO-(*R*)-SO and (*R*)-TFO-(*S*)-SO, and using the intensities of the transitions, determine the enantiomeric excess (ee) satisfactorily [the sample has an ee of 47.2 ± 0.4% (*S*), while the chiral tag experiment gives an ee of 46.7 ± 0.2% (*S*)]. In another study, TFO plays the role of a tag as well as an analyte (a "self-tagging" experiment). The presence of both enantiomers allows the formation of homochiral as well as heterochiral $(TFO)_2$. We have successfully analyzed the spectra of two isomers of homochiral $(TFO)_2$.[11] The lowest-energy heterochiral $(TFO)_2$ is predicted to have no dipole moment, and as a result, it is microwave-silent. Indeed, despite an extensive spectral search, we are not able to identify any heterochiral isomers.

While we are conducting further experiments to continue to explore the usefulness of TFO as a chiral tag, it is also important

Received: May 30, 2023
Revised: June 30, 2023

to examine other tags, as different analytes may interact better with some tags and/or produce dimer spectra with them that are easier to analyze than others. We therefore turn to two analogous fluoromethyl oxiranes: 3-fluoro-1,2-epoxypropane [2-(fluoromethyl)oxirane or FO] and 3,3-difluoro-1,2-epoxypropane [2-(difluoromethyl)oxirane or DFO]. The structures of the lowest-energy FO, DFO, and TFO monomers are similar (two higher-energy conformers of FO have also been reported[12]), yet their complexes with argon show two different motifs.[1−3] We use argon as a buffer gas in our molecular beam to allow repeated formation and dissociation of molecular complexes; thus, each observed argon-fluoromethyl oxirane complex most likely represents the lowest-energy isomer.

Argon interacts with DFO and TFO in a similar manner: using the three-membered epoxy ring as a reference plane, oriented so that the fluoromethyl group is below it, argon lies practically above the O atom, interacting most strongly with it and somewhat less so with the two C atoms in the ring.[2,3] This is the same binding mode observed in the argon complex of the unsubstituted epoxide, ethylene oxide.[13] In the presence of only one F atom in the fluoromethyl group, however, the binding motif of Ar to FO is very different. This time, Ar is off to one side of the ring, interacting with the O and C (the one connected to the CFH_2 group) atoms in the ring and also with the F atom.[1] To understand the different binding modes, we map the electrostatic potential of each epoxide onto its total electron density surface [calculated at the MP2/6-311++G(2d,2p)] level.[1] These mapped surfaces reveal that the most negative atom in all three epoxides is O; thus, it is not surprising that both binding motifs involve an Ar−O interaction. As the number of F atoms increases in the fluoromethyl group, the nucleophilicity of these atoms decreases. The only F atom in FO is very nucleophilic (comparable to that of the O atom in the molecule); therefore, it also forges an interaction with argon. The F atoms in DFO and TFO, on the other hand, are much less nucleophilic and as such, their interactions with argon are not expected to be particularly strong; this is perhaps the reason why this binding mode is not observed for these molecules under our experimental conditions. Of course, attractive and repulsive forces are delicately balanced in intermolecular interactions. Theoretical calculations at the MP2/6-311++G(2d,2p) level show that both modes of argon binding correspond to potential minima for each of these three epoxides, and the energies for these two modes in each argon complex of FO, DFO, and TFO may be too similar (differing in each case by no more than 20 cm^{-1}, that is, 0.25 kJ mol^{-1}) to make the energy ordering reliable. In fact, in the case of Ar−FO, the experimentally observed motif does not agree with the theoretically predicted energy ordering.[1]

Given the two different binding modes observed in these argon-fluoromethyl oxirane complexes, we wish to examine the oxiranes to understand further how they participate in intermolecular interactions and hence, their usefulness as chiral tags. We especially would like to examine several questions: (1) Does the computational method we currently use satisfactorily predict the lowest-energy complex formed by each tag? (2) More fundamentally, how does the presence of different numbers of F atoms in FO, DFO, and TFO affect the ability of these tags to interact with more complicated binding partners? We report our results of two self-tagging studies here, the investigation of the binding modes of $(FO)_2$ and $(DFO)_2$, and compare them to that of $(TFO)_2$.

2. THEORETICAL CALCULATIONS

To explore the conformational landscape in each of the oxirane dimers, we employ the same theoretical methods as those we used previously for the two dimers, $(TFO)_2$ and TFO-SO. We consider all different combinations of the conformers of each oxirane. Applying the artificial bee colony algorithm with the ABCluster program developed by Zhang and Dolg,[14,15] we rapidly identify 28−30 isomers on the potential energy surface that describes the interactions between the various conformational possibilities for the subunits in heterochiral and homochiral $(FO)_2$ and in heterochiral and homochiral $(DFO)_2$. Each isomer is then optimized using density functional theory (DFT), as implemented in Gaussian 16.[16] Specifically, we use the B3LYP functional and the def2-TZVP basis set[17] with the addition of D3 dispersion correction with Becke−Johnson (BJ) damping.[18] All structural parameters, including those of the subunits, are fully relaxed, and harmonic correction is used to give the zero-point energy (all energies reported in the following are zero-point energies). From the isomers of each dimer identified by ABCluster, we obtain 14−17 unique structures after the DFT calculations. The lowest-energy dimers are typically formed by the lowest-energy conformers of FO and DFO.

The lowest-energy heterochiral isomers of $(FO)_2$ and $(DFO)_2$ each have an inversion center; thus, they are nonpolar and have no microwave spectra (Figure 1). The stabilization of these

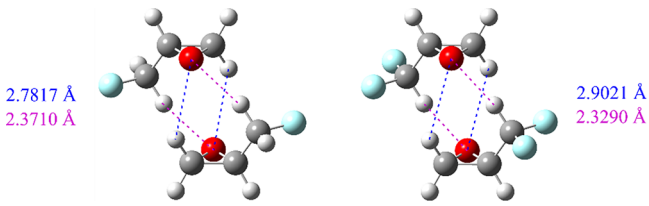

Figure 1. Lowest zero-point energy isomers (using B3LYP-GD3BJ/def2-TZVP) of heterochiral $(FO)_2$ (left) and heterochiral $(DFO)_2$ (right). The most significant intermolecular distances are color coded for easy visualization.

symmetric arrangements is not surprising: the enantiomeric subunits can forge equivalent interactions with each other in each dimer; as such, the electrostatic interactions can be maximized while steric strain can be minimized in the complex. These equivalent interactions in both $(FO)_2$ and $(DFO)_2$ involve the most nucleophilic atom in these oxiranes, O, and H atoms connected to C-1 and C-3, respectively (the atomic positions of these dimers in their principal axis systems are available as Supporting Information). Other heterochiral isomers of $(FO)_2$ are much higher in energy, by at least 156 cm^{-1} or 1.86 kJ mol^{-1}, compared to the lowest-energy structure. The energy gap between the lowest-energy and other heterochiral isomers of $(DFO)_2$ goes up to at least 265 cm^{-1} or 3.17 kJ mol^{-1}. Because the rotational temperature in our molecular beam is only several kelvins, these higher-energy isomers are not likely to be accessible. We are fully aware that intermolecular interactions are too subtle to expect that theoretical calculations will provide energy values accurate to several kJ mol^{-1}, but despite extensive searches, we are not able to observe higher-energy heterochiral dimers of either $(FO)_2$ or $(DFO)_2$.

Each of these most stable heterochiral dimers is also lower in energy than its most stable homochiral counterpart, by 11 cm^{-1}

https://doi.org/10.1021/acs.jpca.3c03643
J. Phys. Chem. A XXXX, XXX, XXX−XXX

(0.13 kJ mol^{-1}) for $(FO)_2$ and by 92 cm^{-1} (1.1 kJ mol^{-1}) for $(DFO)_2$. Three isomers each of homochiral $(FO)_2$ and $(DFO)_2$ have relative energies less than 100 cm^{-1} (1.20 kJ mol^{-1}); these energies are listed in Table 1 and their structures, labeled (i–iii)

Table 1. Relative Zero-Point Energies in cm^{-1} and in kJ mol^{-1} for the Three Lowest-Energy Isomers of Homochiral $(FO)_2$ and of Homochiral $(DFO)_2$ Using Different Levels of Theory and Basis Sets[a]

	B3LYP def2-TZVP		B3LYP 6-311++G (p,d)		B3LYP 6-311++G (2p,2d)		MP2 6-311++G (2p,2d)	
	cm^{-1}	kJ mol^{-1}	cm^{-1}	kJ mol^{-1}	cm^{-1}	kJ mol^{-1}	cm^{-1}	kJ mol^{-1}
				$(FO)_2$				
(i)	0	0	0	0	0	0	0	0
(ii)	39	0.46	23	0.28	32	0.39	63	0.75
(iii)	62	0.75	39	0.47	51	0.61	180	2.16
				$(DFO)_2$				
(i)	0	0	0	0	0	0	0	0
(ii)	43	0.52	6	0.08	50	0.60	93	1.12
(iii)	67	0.80	33	0.40	82	0.98	223	2.66

[a]GD3BJ dispersion is included in calculations that use the B3LYP model.

in order of increasing energy, are shown in Figure 2 (the atomic positions of these isomers in their principal axis systems are

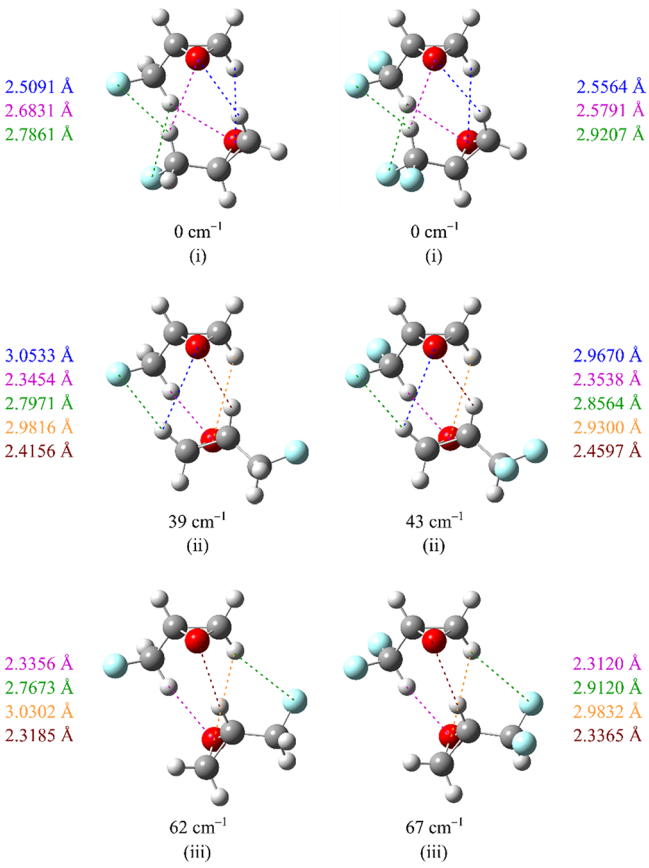

Figure 2. Three isomers with lowest zero-point energies (using B3LYP-GD3BJ/def2-TZVP) for homochiral $(FO)_2$ (left) and for homochiral $(DFO)_2$ (right). The most significant intermolecular distances are color coded for easy visualization.

available as the Supporting Information). To investigate what level of theory is more adequate for these species, we also optimized these six isomers using different levels of theory and basis sets, namely, B3LYP with 6-311++G(p,d) and 6-311++G(2p,2d), both with GD3BJ dispersion, and MP2 with 6-311++G(2p,2d). The harmonically corrected zero-point energies are listed in Table 1. Indeed, all four methods show the same energy ordering for homochiral $(FO)_2$ and $(DFO)_2$.

The lowest-energy homochiral $(FO)_2$, $(FO)_2$-i, has a C_2 axis and two sets of equivalent interactions: O interacting with two hydrogen atoms connected to C-1 and C-3, respectively, and an F atom interacting with an H atom connected to C-3 (Figure 2). The reason why the six interactions do not stabilize the homochiral complex as much as the four interactions in the heterochiral complex (Figure 1) is apparent when the interaction lengths are compared. The two sets of equivalent O···H interactions in each complex involve the same H atoms. The one connected to C-3 should be more electropositive because of its proximity to the F atom than the one connected to C-1. Without the CF_3 groups near each other, the O···H(C-3) interaction in the heterodimer is allowed to be very short (2.3710 Å, as opposed to 2.6831 Å in the homochiral dimer) and, hence, strong. The proximity of the CF_3 groups allow two F···H(C3) interactions, but a length of 2.7861 Å suggests a fairly weak intermolecular bond. Much of the same can be said for the lowest-energy heterochiral $(DFO)_2$ (Figure 1) and lowest-energy homochiral $(DFO)_2$, $(DFO)_2$-i (Figure 2). This time, the O···H(C-3) interaction in the heterochiral species is 2.3290 Å [slightly shorter than its heterochiral $(FO)_2$ counterpart but more significantly so than the 2.5791 Å length in homochiral $(DFO)_2$], and it appears to be the interaction that makes the heterochiral $(DFO)_2$ more stable than homochiral $(DFO)_2$. It is interesting to note that the next higher-energy homochiral isomer of $(FO)_2$ and that of $(DFO)_2$ likewise share structural similarities; the same is true for the pair of isomers still higher in energy (Figure 2). Using the same four model chemistries mentioned previously, the rotational constants and dipole moment components are calculated at the equilibrium structures for the lowest-energy homochiral $(FO)_2$ and $(DFO)_2$ isomers and tabulated in Table 2. Because of the symmetry of each of these dimers, the only nonzero dipole moment component is along the *b* inertial axis, which is also the C_2 symmetry axis for each dimer (Figure 2, top).

3. EXPERIMENT

Rotational transitions of $(FO)_2$ and $(DFO)_2$ are observed in the broadband, chirped pulse Fourier transform microwave (CP-FTMW) spectra previously obtained for and described in our reports on FO/Ar-FO[1] and DFO/Ar-DFO,[2] respectively. Briefly, vapor of the relevant oxirane is entrained in argon and introduced into a spectrometer[19−21] via expansion through two pulsed valves, each with a 0.8 mm orifice. The 5.6−18.1 GHz spectrum is obtained in three separately acquired segments by polarization with a 4 μs chirped pulse with 20−25 W of power followed by 50 Gs s^{-1} digitization of the resulting free induction decay (FID). For FO, the FID is digitized for 20 μs, which after averaging is Fourier transformed to give a frequency domain spectrum with a resolution element of 11.92 kHz, typical line widths (FWHM) of 125 kHz, and allows us to assign line centers with an estimated measurement uncertainty of 5 to 10 kHz. For DFO, only 10 μs of the FID is recorded resulting in a 23.84 kHz resolution element, line widths of 225 kHz, and an estimated measurement uncertainty of 10 to 15 kHz. As noted in the earlier

https://doi.org/10.1021/acs.jpca.3c03643
J. Phys. Chem. A XXXX, XXX, XXX−XXX

Table 2. Rotational Constants and the *b* Dipole Moment Components[a] Predicted Using Different Levels of Theory and Basis Sets[b] for $(FO)_2$ and $(DFO)_2$[c]

	B3LYP def2-TZVP		B3LYP 6-311++G(p,d)		B3LYP 6-311++G(2p,2d)		MP2 6-311++G(2p,2d)		
	theory	exp. − theory	theory	exp. − theory	theory	exp. − theory	theory	exp. − theory	experiment[d]
					$(FO)_2$				
A/MHz	1485.4	11.9	1477.1	20.2	1480.6	16.7	1497.4	−0.11	1497.31344(36)
B/MHz	944.6	−18.1	947.1	−20.5	940.8	−14.2	981.2	−54.7	926.58964(31)
C/MHz	652.3	−7.7	652.4	−7.8	650.1	−5.4	673.2	−28.6	644.61117(13)
$\lvert\mu_b\rvert$/D	2.92		3.29		3.08		3.00		
					$(DFO)_2$				
A/MHz	1169.5	7.9	1175.3	2.1	1164.9	12.4	1170.6	6.7	1177.32680(60)
B/MHz	572.6	−4.1	568.3	0.2	578.3	−9.8	602.0	−33.5	568.49295(41)
C/MHz	471.1	−4.1	472.6	−5.6	475.7	−8.8	489.5	−22.5	466.98133(25)
$\lvert\mu_b\rvert$/D	4.24		4.69		4.42		4.36		

[a]The *a* and *c* dipole moment components are zero. [b]GD3BJ dispersion is included in calculations that use the B3LYP model. [c]The experimental rotational constants, derived from the *A*-reduced Hamiltonian, are also listed for comparison. [d]These constants are derived from the Watson *A*-reduced Hamiltonian.

reports,[1,2] significantly fewer FIDs were averaged for the DFO spectrum (72,000 to 78,000) than for the FO spectrum (450,000 to 1,713,000).

4. SPECTRAL ANALYSIS

We have observed 74−76 *b*-type transitions each for homochiral $(FO)_2$ and $(DFO)_2$, sampling *J* from 2 to at least 13 and K_a from 0 to at least 6. We have searched for *a*- and *c*-type transitions but are not able to locate any, consistent with the theoretical predictions for and symmetry of the most stable species. Figure 3

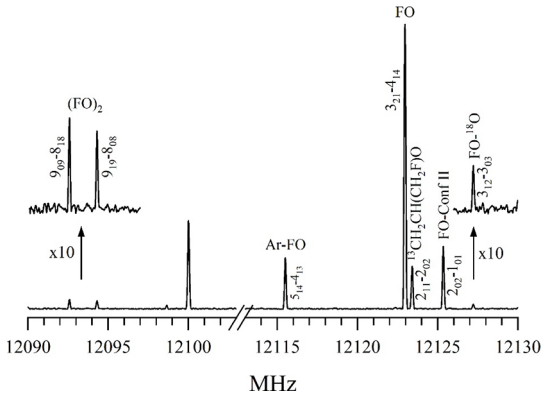

Figure 3. Forty megahertz portion of the spectrum taken with FO in Ar showing spectral lines due to the three isotopologues of the most stable conformer of FO and a less stable conformer of FO, Ar−FO, and $(FO)_2$.

shows a portion of the spectrum taken with FO in argon in which two transitions of homochiral $(FO)_2$ are observed, together with several transitions due to the isotopologues of the most stable conformer of FO and Ar−FO[1,12] and one due to a less stable conformer of FO, conformer II.[12] The transition intensities of the homochiral dimer are similar to the ^{18}O isotopologue of the most stable conformer of FO. Using DFO in argon, Figure 4 shows transitions due to homochiral $(DFO)_2$, as well as four isotopologues of DFO and Ar-DFO. This time, the spectral lines for $(DFO)_2$ have similar intensities as those for Ar-DFO and the ^{13}C isotopologues of DFO.

Spectral assignments of homochiral $(FO)_2$ and $(DFO)_2$ are performed with Kisiel's AABS program,[22] and the transitions are analyzed using both Watson *A*- and *S*-reduced Hamiltonians,[23−25] each in the I^r representation, and Pickett's nonlinear

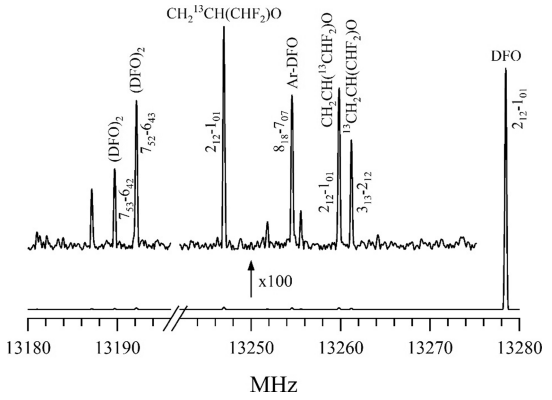

Figure 4. One hundred megahertz portion of the spectrum taken with DFO in Ar showing spectral lines due to four isotopologues of DFO, Ar-DFO, and $(DFO)_2$.

least squares SPFIT program.[26] For each species and for each Hamiltonian, we obtain three rotational constants and five quartic centrifugal constants (Table 3). The rms uncertainties of these fits, 4 kHz for $(FO)_2$ and 9 kHz for $(DFO)_2$, are reasonable, within a portion of a linewidth. The rms uncertainties also reflect the different FID lengths and resulting measurement uncertainties for the two species. The longer (20 μs) FID length for $(FO)_2$ provides a more precise determination of the transition frequency and a smaller rms than does the shorter (10 μs) FID used in obtaining the $(DFO)_2$ spectrum (tables of observed and calculated transition frequencies with assignments for these species fitted to the *A*-reduced Hamiltonian are available as the Supporting Information). As expected, the corresponding rotational constants from the two Hamiltonians are practically the same, differing by less than 0.0008% for $(FO)_2$ and less than 0.0003% for $(DFO)_2$. With an asymmetry parameter of −0.71 for $(DFO)_2$, the species is less of an asymmetric top than $(FO)_2$, which has an asymmetry parameter of −0.34.

5. DISCUSSION

Our experimental work is well guided by theory: we are able to use the theoretical rotational constants for the lowest-energy isomers to assign the spectra for homochiral $(FO)_2$ and $(DFO)_2$. The DFT method using any one of the three basis sets works particularly well (Table 2). In general, the values for the *A*

https://doi.org/10.1021/acs.jpca.3c03643
J. Phys. Chem. A XXXX, XXX, XXX−XXX

Table 3. Spectroscopic Constants (in MHz, Unless Otherwise Noted), Fitted, Respectively, to the Watson *A*-Reduced and *S*-Reduced Hamiltonians, for $(FO)_2$ and $(DFO)_2$[a]

A-reduction	$(FO)_2$	$(DFO)_2$	*S*-reduction	$(FO)_2$	$(DFO)_2$
A	1497.31344(36)	1177.32680(60)	A	1497.31497(36)	1177.32693(60)
B	926.58964(31)	568.49295(41)	B	926.58301(30)	568.49155(39)
C	644.61117(13)	466.98133(25)	C	644.61659(13)	466.98263(24)
$\Delta_J/10^{-3}$	0.5681(23)	0.1991(20)	$D_J/10^{-3}$	0.2694(16)	0.1732(17)
$\Delta_{JK}/10^{-3}$	4.6569(79)	0.5700(99)	$D_{JK}/10^{-3}$	6.4499(74)	0.725(10)
$\Delta_K/10^{-3}$	−5.0457(82)	−0.577(12)	$D_K/10^{-3}$	−6.5400(83)	−0.706(12)
$\delta_J/10^{-3}$	0.1671(11)	0.0474(10)	$d_1/10^{-3}$	−0.1670(11)	−0.0474(10)
$\delta_K/10^{-3}$	3.0130(97)	0.673(19)	$d_2/10^{-3}$	−0.14923(48)	−0.01294(37)
rms/kHz	4.40	8.91	rms/kHz	4.44	8.91
	$(FO)_2$			$(DFO)_2$	
no. of transitions	76			74	
J range	2−13			2−14	
K_a range	0−6			0−7	

[a] 1σ standard deviations in the parameters are given in parentheses.

constant are underestimated (by 2−20 MHz) but those for the *B* and *C* constants are overestimated (by 4−20 MHz) [the only exception is that the *B* value calculated for $(DFO)_2$ with the 6-311++G(p,d) basis set is underestimated by a remarkably small amount, 0.2 MHz]. For $(FO)_2$, both def2-TZVP and 6-311++G(2p,2d) basis sets give somewhat better predictions than the 6-311++G(p,d) basis set, but for $(DFO)_2$, the 6-311++G(p,d) basis set gives the best prediction, and def2-TZVP is better than 6-311++G(2p,2d). It appears that each basis set gives somewhat better predictions for the heavier $(DFO)_2$ than for $(FO)_2$. The MP2/6-311++G(2p,2d) level of theory, however, did not do as well compared to the DFT method. While it predicts the *A* constants for the two species to within 7 MHz, the *B* and *C* constants are overestimated by 23−55 MHz. The *A* rotational constant is more sensitive to the relative orientation of the subunits about the *a*-axis (which is very well approximated by the line joining the centers of mass of the two subunits), while the *B* and *C* rotational constants are more sensitive to the intermolecular distance (and the *A* rotational constant less so). This indicates that the MP2 level of theory does very well with the mass distribution about the *a*-axis but overestimates the intermolecular interactions, which is a known problem, resulting in a shorter intermolecular distance and smaller moments of inertia about the *b*- and *c*-axes. The inherent high-resolution nature of our technique can be greatly facilitated by theory that gives a balance of high accuracy and time economy; as such, in this application, the more time-consuming MP2 level of theory does not offer an advantage to us.

To examine how the number of F atoms in the fluoromethyl group affects the nature of intermolecular interactions in the homodimers, we compare the lowest-energy homodimers of $(FO)_2$ and $(DFO)_2$ in this work with their $(TFO)_2$ counterpart. In the presence of one or two F atoms, the fluoromethyl group in one subunit points toward the other subunit, making possible two F···H interactions (Figure 2) as well as four O···H interactions (with lengths of 2.5−2.7 Å). The F···H interactions in $(FO)_2$ are shorter and thus stronger than those in $(DFO)_2$. This is consistent with our finding from the mapped electrostatic surfaces of these species that the F atoms in FO is more nucleophilic than those in DFO.[1] When three F atoms are present, however, there is no longer any H atom available in the trifluoromethyl group to form similar F···H interactions in the homodimer. In fact, for both the homochiral and heterochiral TFO dimers, the trifluoromethyl group in each TFO subunit points away from the other subunit (Figure 5) and the subunits are bound together by four O···H interactions, with lengths of

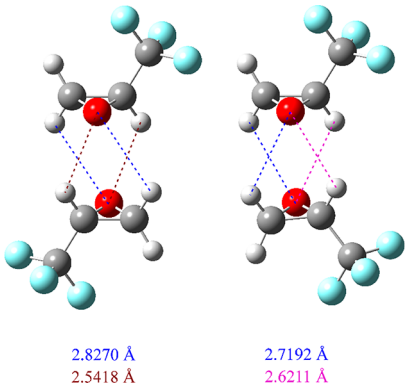

Figure 5. Heterochiral (left) and homochiral (right) isomers of $(TFO)_2$ with lowest zero-point energies (using B3LYP-GD3BJ/def2-TZVP).

2.5−2.8 Å, similar to those found in their $(FO)_2$ and $(DFO)_2$ counterparts. However, in $(TFO)_2$, the hydrogen atoms involved in the interactions are all ring hydrogens, while for $(FO)_2$ and $(DFO)_2$, one ring hydrogen and one fluoromethyl hydrogen from each subunit interact with the oxygen atom on the other. This configuration is not surprising. The F atoms in TFO are even less nucleophilic than those in DFO[1] and therefore, they are unlikely to interact strongly with their dimeric partner. Furthermore, the trifluoromethyl groups are bulky and would cause severe steric effects if they were to point toward each other in the dimer.[11]

To explore if the homochiral and heterochiral isomers of $(TFO)_2$ may assume structures similar to those of $(FO)_2$ or $(DFO)_2$, we start the dimer at each of these configurations and try to locate a minimum nearby using B3LYP/def2-TZVP with GD3BJ empirical dispersion. We are able to find such a configuration for the heterochiral $(TFO)_2$, but it is 244 cm^{-1} or 2.92 kJ mol^{-1} higher in energy than the most stable isomer (Figure 5), but we are unsuccessful in finding a similar configuration for the homochiral dimer.

It is instructive to compare the observed and predicted isomers of $(FO)_2$ and $(DFO)_2$ with those of their nonfluorinated counterpart, the propylene oxide dimer, $(PO)_2$,[27] as we did

https://doi.org/10.1021/acs.jpca.3c03643
J. Phys. Chem. A XXXX, XXX, XXX−XXX

Table 4. Contributions to SAPT Binding Energy (in kJ mol^{-1} and % of Total Stabilization Energy[a]) for Three Lowest-Energy Homochiral and the Lowest-Energy Heterochiral Isomers for $(FO)_2$ and $(DFO)_2$ and the Lowest-Energy Homochiral and Heterochiral $(TFO)_2$

	electrostatics		induction		dispersion		exchange		SAPT
	kJ mol^{-1}	%	kJ mol^{-1}	%	kJ mol^{-1}	%	kJ mol^{-1}	%	kJ mol^{-1}
					$(FO)_2$				
(i)	−28.50	50.68	−6.37	11.33	−21.37	37.99	26.51	−47.13	−29.74
(ii)	−29.78	55.02	−6.05	11.18	−18.30	33.80	25.56	−47.21	−28.58
(iii)	−31.33	56.11	−6.83	12.24	−17.67	31.65	28.54	−51.11	−27.30
heterochiral	−31.76	54.40	−6.56	11.23	−20.07	34.37	27.06	−46.35	−31.33
					$(DFO)_2$				
(i)	−27.05	50.56	−5.82	10.88	−20.64	38.57	25.28	−47.23	−28.24
(ii)	−28.42	54.79	−5.46	10.53	−17.99	34.68	23.97	−46.20	−27.91
(iii)	−29.95	56.20	−6.33	11.87	−17.01	31.93	26.97	−50.61	−26.32
heterochiral	−32.75	55.38	−6.70	11.33	−19.69	33.29	27.41	−46.35	−31.72
					$(TFO)_2$				
homochiral	−21.55	51.37	−3.78	9.00	−16.62	39.63	17.92	−42.72	−24.03
heterochiral	−22.74	52.69	−3.96	9.17	−16.46	38.14	18.53	−42.93	−24.62

[a]The stabilization energy is the sum of electrostatics, induction, and dispersion energies. Percentages are relative to this total stabilization energy. In the case of exchange energy, the negative percentage indicates that it is destabilizing.

earlier with the TFO dimer.[11] All of the observed PO dimers contain at least one hydrogen bond between a methyl group hydrogen and a ring oxygen, in common with those observed here for FO and DFO. However, the effects of fluorine substitution can be seen in multiple ways. The lowest-energy isomers predicted for heterochiral $(FO)_2$ and $(DFO)_2$ are analogous to the similarly nonpolar and unobserved *RS*1 isomers of $(PO)_2$, with two symmetrically equivalent hydrogen bonds forming between a methyl group hydrogen atom on one monomer and the ring oxygen of the other and an additional two forming between a hydrogen atom of the ring $-CH_2$ group of one monomer and the ring oxygen of the other, which is termed H3H2*R*-H3H2*S* in ref 27. Interestingly, despite the presence of fluorine atoms in FO and DFO, there are no hydrogen bonds involving fluorine atoms in this lowest-energy heterochiral dimer.

For the homochiral PO dimer, the isomer predicted to have the lowest energy, *RR*1, was also predicted to have very small dipole moment components and was not observed.[27] The presence of the fluorine atoms in $(FO)_2$ and $(DFO)_2$ results in rather large dipole moments for their respective analogous H3H2*R*-H3H2*R* lowest-energy isomers, and these are the only isomers observed in the argon expansion used here. One of the observed isomers of homochiral $(PO)_2$, *RR*4 (H3H2*R*-H2H1*R*), is structurally similar to the higher-energy isomer (ii) of $(FO)_2$ and $(DFO)_2$. However, in $(PO)_2$, this isomer is higher in energy than isomer *RR*2 (H3H2*R*-H3H1*R*). We attribute the lowering in $(FO)_2$ and $(DFO)_2$ to the presence of a hydrogen bond between one of the fluoromethyl fluorine atoms and a $-CH_2$ ring hydrogen, which is not possible in $(PO)_2$. A similarly formed hydrogen bond in isomer (iii) of $(FO)_2$ and $(DFO)_2$ leads to the stabilization of this isomer that has no $(PO)_2$ analogue.

We can examine how the various contributions to the intermolecular interactions—electrostatic, induction, dispersion, and exchange—affect the stability of the FO, DFO, and TFO dimers using symmetry-adapted perturbation theory (SAPT)[28] as implemented in the PSI4 program package,[29] choosing the def2-TZVP basis. The results are summarized in Table 4 and Figures 6 and 7. The greatest contribution to stability for each species comes from electrostatics (>50%),

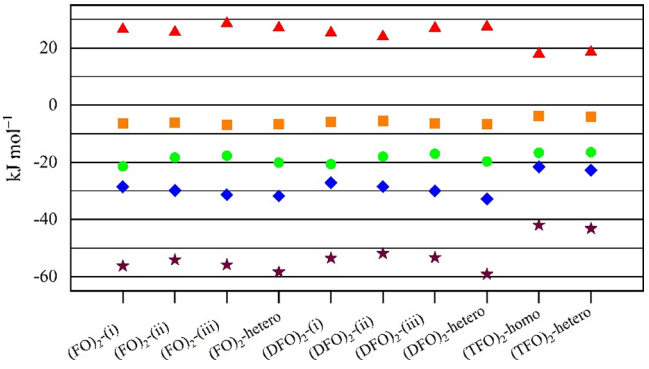

Figure 6. Contribution to SAPT binding energy from exchange (red triangles), induction (orange squares), dispersion (green circles), and electrostatics (blue diamonds), together with the total stabilization energy (sum of electrostatics, dispersion, and induction energies, brown stars). For $(FO)_2$ and $(DFO)_2$, the three lowest-energy homochiral and the lowest-energy heterochiral species are shown. For $(TFO)_2$, only the lowest-energy homochiral and heterochiral species are shown.

followed by dispersion (32−40%) and then induction (9−12%). The exchange energy is repulsive, and its magnitude is ∼43−51% of the stabilization energy (that arises from the other three contributions). Let us consider first the lowest-energy, microwave-silent heterochiral dimers of FO, DFO, and TFO. The first two species are lower in energy by 6.7 and 7.1 kJ mol^{-1}, respectively, than $(TFO)_2$. For $(FO)_2$ and $(DFO)_2$, the SAPT energy for heterochiral species is lower than that for the lowest-energy homochiral species; specifically, by 1.6 and 3.5 kJ mol^{-1}, respectively. The major factor for this lowering is due to more favorable electrostatics contributions. As described earlier, in the homochiral species, the bulky fluoromethyl groups are near each other, preventing short intermolecular interactions between O, the most nucleophilic atom in one subunit, and H atoms in the other subunit. The steric effects are lessened for the heterochiral species where the fluoromethyl groups can be located away from each other (Figures 1 and 2). In the case of $(TFO)_2$, because the fluoromethyl groups in both heterochiral and homochiral dimers are located far from each other, the electrostatics contribution for both species are similar. Nevertheless, taking all

https://doi.org/10.1021/acs.jpca.3c03643
J. Phys. Chem. A XXXX, XXX, XXX−XXX

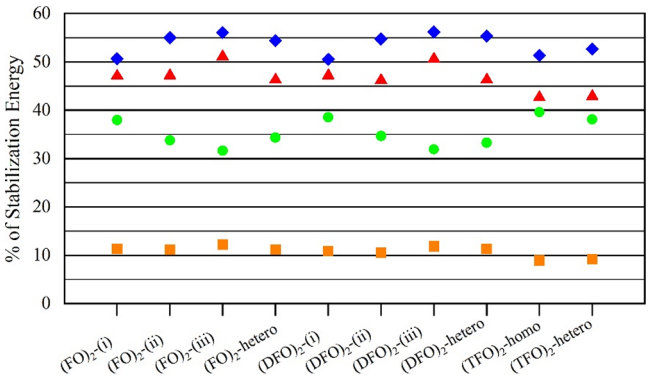

Figure 7. Contribution to SAPT binding energy from electrostatics (blue diamonds), exchange (red triangles), dispersion (green circles), and induction (orange squares), each as a percentage of the total stabilization energy. Note the exchange energy is destabilizing; only the magnitude of the percentage is expressed. For $(FO)_2$ and $(DFO)_2$, the three lowest-energy homochiral and the lowest-energy heterochiral species are shown. For $(TFO)_2$, only the lowest-energy homochiral and heterochiral species are shown.

contributions together, the heterochiral species is slightly more stabilized by 0.6 kJ mol^{-1}.

In the case of the three lowest-energy isomers of the homochiral species, the induction contributions for these isomers of the same dimer [$(FO)_2$ or $(DFO)_2$] are quite small (only several kJ mol^{-1}) and also similar, differing by at most 0.51 kJ mol^{-1}. The contributions from electrostatics (approximately 30 kJ mol^{-1}) and dispersion (approximately 20 kJ mol^{-1}) are greater. While isomer (iii) is most stabilized by the electrostatics contribution, followed by isomer (ii), which in turn is followed by isomer (i) for each dimer, the order of stabilization provided by dispersion is reversed. Additionally, isomer (iii) is destabilized more by the exchange contribution. Taken together, isomer (i) is the lowest in energy for each dimer; specifically, for $(FO)_2$, the SAPT energy for isomer (i) is 1.2 and 2.4 kJ mol^{-1} lower than those for isomers (ii) and (iii), respectively, and for $(DFO)_2$, the SAPT energy for isomer (i) is 0.3 and 1.9 kJ mol^{-1} lower than those for isomers (ii) and (iii), respectively. Isomer (i) is the only homochiral dimer observed for each of $(FO)_2$ and $(DFO)_2$. In fact, the SAPT energy for isomer (i) of $(FO)_2$ is 1.5 kJ mol^{-1} lower than that of $(DFO)_2$, which in turn is 4.2 kJ mol^{-1} lower than that for the lowest-energy homochiral $(TFO)_2$ observed. In the case of this $(TFO)_2$ homodimer, although the destabilizing exchange energy is the smallest compared to isomer (i) of $(FO)_2$ and isomer (i) of $(DFO)_2$, the dispersion contribution and, more noticeably, the electrostatics contribution are the least of all.

One of the interesting aspects of Figure 6 is that the SAPT energies of the three isomers of homochiral $(FO)_2$ or $(DFO)_2$ are very similar; yet under argon expansion, we are only able to observe one of them [in the case of $(TFO)_2$, two homochiral isomers are observed in the argon expansion]. If the FO monomer or the DFO monomer can form only one observable isomeric complex with each of a pair of enantiomeric analytes in an argon expansion, it will greatly reduce spectral congestion and, as such, make them more useful as chiral tags. Of course, further experimentation is necessary to be able to draw such a conclusion.

6. CONCLUSIONS

Quantum chemistry characterization of the heterochiral and homochiral gas-phase homodimers of FO and DFO reveals several low energy isomers for each. In the case of the heterochiral homodimers, the lowest-energy form of each possesses a center of inversion. Consequently, the dipole moment vanishes, and they do not have a microwave rotational spectrum. Additionally, the higher-energy forms, which are polar, apparently are sufficiently high in energy that they are not populated under the conditions of our experiment, as no spectra for either of the heterochiral dimers are found. However, spectra are obtained for one isomer each of the homochiral dimers of FO and DFO. Upon analysis, these are identified as corresponding to the lowest-energy forms predicted by theory. Unlike the homodimers of the similar molecule TFO in which the fluoromethyl groups are positioned on the outside of the dimer, presumably to minimize steric clash, in the lowest-energy forms of $(FO)_2$ and $(DFO)_2$, the fluoromethyl groups are located between the two subunits where they participate in the binding and contribute to additional stabilization. SAPT calculations show significantly greater electrostatic (~27 to 33 kJ mol^{-1} versus ~23 kJ mol^{-1}) but more similar dispersion stabilization (~20 kJ mol^{-1} versus ~17 kJ mol^{-1}) in $(FO)_2$ and $(DFO)_2$ as compared to $(TFO)_2$, while $(TFO)_2$ has only ~70% of the exchange destabilization (18 kJ mol^{-1}) found in $(FO)_2$ and $(DFO)_2$ (25 to 27 kJ mol^{-1}). On balance, the SAPT results show $(FO)_2$ and $(DFO)_2$ are both more strongly bound than $(TFO)_2$, although the difference in binding energy between the homo- and heterochiral dimers is greater in $(FO)_2$ and $(DFO)_2$ than $(TFO)_2$.

Our assignment and analysis of the spectra for these species were greatly facilitated by the use of rather modest quantum chemistry methods. In particular, the equilibrium rotational constants predicted using DFT (augmented with empirical dispersion) provided good estimates of the zero-point averaged rotational constants observed in the spectra and showed little basis set dependence. This will be valuable in applications of the chiral tagging method by not needing the use of more realistic, but expensive, methods that would then require the calculation and application of vibrational corrections to predict the spectra of diastereomeric chiral tag-analyte pairs. These modest calculations, admittedly with the inclusion of harmonic zero-point corrections, also did surprisingly well in identifying the lowest-energy forms of the dimers.

■ ASSOCIATED CONTENT

Supporting Information

The Supporting Information is available free of charge at https://pubs.acs.org/doi/10.1021/acs.jpca.3c03643.

Tables of observed and calculated transition frequencies for the observed homochiral heterodimers of FO and DFO, the atomic coordinates for the theoretical structures shown in Figures 1 and 2, and the complete citation for Gaussian 16 (ref 16) (PDF)

■ AUTHOR INFORMATION

Corresponding Authors

Mark D. Marshall − *Department of Chemistry, Amherst College, Amherst, Massachusetts 01002-5000, United States;* orcid.org/0000-0002-4052-4840; Phone: (413) 542-2006; Email: mdmarshall@amherst.edu; Fax: (413) 542-2735

https://doi.org/10.1021/acs.jpca.3c03643
J. Phys. Chem. A XXXX, XXX, XXX−XXX

Helen O. Leung − *Department of Chemistry, Amherst College, Amherst, Massachusetts 01002-5000, United States;* orcid.org/0000-0001-5241-5775; Phone: (413) 542-2660; Email: hleung@amherst.edu; Fax: (413) 542-2735

Complete contact information is available at: https://pubs.acs.org/10.1021/acs.jpca.3c03643

Notes

The authors declare no competing financial interest.

■ ACKNOWLEDGMENTS

This material is based on work supported by the National Science Foundation under Grant No. CHE-1856637

■ REFERENCES

(1) Leung, H. O.; Marshall, M. D.; Stuart, D. J. Microwave Spectrum and Molecular Structure of 3-Fluoro-1,2-Epoxypropane and the Unexpected Structure of Its Complex with the Argon Atom. *J. Phys. Chem. A* **2020**, *124*, 1798−1810.

(2) Marshall, M. D.; Leung, H. O. The Microwave Spectrum and Molecular Structure of 3,3-Difluoro-1,2-Epoxypropane and Its Complex with the Argon Atom. *J. Mol. Spectrosc.* **2018**, *350*, 18−26.

(3) Marshall, M. D.; Leung, H. O.; Wang, K.; Acha, M. D. Microwave Spectrum and Molecular Structure of the Chiral Tagging Candidate, 3,3,3-Trifluoro-1,2-Epoxypropane and Its Complex with the Argon Atom. *J. Phys. Chem. A* **2018**, *122*, 4670−4680.

(4) Borho, N.; Xu, Y. Lock-and-Key Principle on a Microscopic Scale: The Case of the Propylene Oxide···Ethanol Complex. *Angew. Chem., Int. Ed.* **2007**, *46*, 2276−2279.

(5) Seifert, N. A.; Pérez, C.; Neill, J. L.; Pate, B. H.; Vallejo-López, M.; Lesarri, A.; Cocinero, E. J.; Castaño, F. Chiral Recognition and Atropisomerism in the Sevoflurane Dimer. *Phys. Chem. Chem. Phys.* **2015**, *17*, 18282−18287.

(6) Evangelisti, L.; Caminati, W.; Patterson, D.; Thomas, J.; Xu, Y.; West, C.; Pate, B. A Chiral Tagging Strategy for Determining Absolute Configuration and Enantiomeric Excess by Molecular Rotational Spectroscopy. *The 72nd International Symposium on Molecular Spectroscopy, Talk RG-03*; Urbana-Champaign, IL, 2017.

(7) Domingos, S. R.; Pérez, C.; Marshall, M. D.; Leung, H. O.; Schnell, M. Assessing the Performance of Rotational Spectroscopy in Chiral Analysis. *Chem. Sci.* **2020**, *11*, 10863−10870.

(8) Pate, B. H.; Evangelisti, L.; Caminati, W.; Xu, Y.; Thomas, J.; Patterson, D.; Pérez, C.; Schnell, M., Quantitative Chiral Analysis by Molecular Rotational Spectroscopy. In *Chiral Analysis*, 2nd ed.; Elsevier: 2018; 679−729.

(9) Sonstrom, R. E.; Neill, J. L.; Mikhonin, A. V.; Doetzer, R.; Pate, B. H. Chiral Analysis of Pantolactone with Molecular Rotational Resonance Spectroscopy. *Chirality* **2022**, *34*, 114−125.

(10) Mills, M. D.; Sonstrom, R. E.; Vang, Z. P.; Neill, J. L.; Scolati, H. N.; West, C. T.; Pate, B. H.; Clark, J. R. Enantioselective Synthesis of Enantioisotopomers with Quantitative Chiral Analysis by Chiral Tag Rotational Spectroscopy. *Angew. Chem., Int. Ed.* **2022**, *61*, No. e202207275.

(11) Marshall, M. D.; Leung, H. O.; Domingos, S. R.; Krin, A.; Schnell, M.; Seifert, N. A.; Xu, Y. J.; Jäger, W. Examining the Gas-Phase Homodimers of 3,3,3-Trifluoro-1,2-Epoxypropane Using Quantum Chemistry and Microwave Spectroscopy. *Phys. Chem. Chem. Phys.* **2022**, *24*, 28495−28505.

(12) Brown, G. G.; Dian, B. C.; Douglass, K. O.; Geyer, S. M.; Pate, B. H. The Rotational Spectrum of Epifluorohydrin Measured by Chirped-Pulse Fourier Transform Microwave Spectroscopy. *J. Mol. Spectrosc.* **2006**, *238*, 200−212.

(13) Moreschini, P.; Caminati, W.; Favero, P. G.; Legon, A. C. Pathways for Inversion in the Oxirane-Argon Complex. *J. Mol. Struct.* **2001**, *599*, 81−87.

(14) Zhang, J.; Dolg, M. Abcluster: The Artificial Bee Colony Algorithm for Cluster Global Optimization. *Phys. Chem. Chem. Phys.* **2015**, *17*, 24173−24181.

(15) Zhang, J.; Dolg, M. Global Optimization of Rigid Molecular Clusters by the Artificial Bee Colony Algorithm. *Phys. Chem. Chem. Phys.* **2016**, *18*, 3003−3010.

(16) Frisch, M. J.; Trucks, G. W.; Schlegel, H. B.; Scuseria, G. E.; Robb, M. A.; Cheeseman, J. R.; Scalmani, G.; Barone, V.; Petersson, G. A.; Nakatsuji, H.; Li, X.; Caricato, M.; Marenich, A.V.; Bloino, J.; Janesko, B.G.; Gomperts, R.; Mennucci, B.; Hratchian, H.P.; Ortiz, J.V.; Izmaylov, A.F.; Sonnenberg, J.L.; Williams-Young, D.; Ding, F.; Lipparini, F.; Egidi, F.; Goings, J.; Peng, B.; Petrone, A.; Henderson, T.; Ranasinghe, D.; Zakrzewski, V.G.; Gao, J.; Rega, N.; Zheng, G.; Liang, W.; Hada, M.; Ehara, M.; Toyota, K.; Fukuda, R.; Hasegawa, J.; Ishida, M.; Nakajima, T.; Honda, Y.; Kitao, O.; Nakai, H.; Vreven, T.; Throssell, K.; Montgomery, Jr., J.A.; Peralta, J.E.; Ogliaro, F.; Bearpark, M.J.; Heyd, J.J.; Brothers, E.N.; Kudin, K.N.; Staroverov, V.N.; Keith, T.A.; Kobayashi, R.; Normand, J.; Raghavachari, K.; Rendell, A.P.; Burant, J.C.; Iyengar, S.S.; Tomasi, J.; Cossi, M.; Millam, J.M.; Klene, M.; Adamo, C.; Cammi, R.; Ochterski, J.W.; Martin, R.L.; Morokuma, K.; Farkas, O.; Foresman, J.B.; Fox, D.J. *Gaussian 16, Revision A.03*; Gaussian, Inc.: Wallingford, CT, 2016.

(17) Weigend, F.; Ahlrichs, R. Balanced Basis Sets of Split Valence, Triple Zeta Valence and Quadruple Zeta Valence Quality for H to Rn: Design and Assessment of Accuracy. *Phys. Chem. Chem. Phys.* **2005**, *7*, 3297−3305.

(18) Grimme, S.; Ehrlich, S.; Goerigk, L. Effect of the Damping Function in Dispersion Corrected Density Functional Theory. *J. Comput. Chem.* **2011**, *32*, 1456−1465.

(19) Marshall, M. D.; Leung, H. O.; Scheetz, B. Q.; Thaler, J. E.; Muenter, J. S. A Chirped Pulse Fourier Transform Microwave Study of the Refrigerant Alternative 2,3,3,3-Tetrafluoropropene. *J. Mol. Spectrosc.* **2011**, *266*, 37−42.

(20) Marshall, M. D.; Leung, H. O.; Calvert, C. E. Molecular Structure of the Argon-(*Z*)-1-Chloro-2-Fluoroethylene Complex from Chirped-Pulse and Narrow-Band Fourier Transform Microwave Spectroscopy. *J. Mol. Spectrosc.* **2012**, *280*, 97−103.

(21) Leung, H. O.; Marshall, M. D.; Messinger, J. P.; Knowlton, G. S.; Sundheim, K. M.; Cheung-Lau, J. C. The Microwave Spectra and Molecular Structures of 2-Chloro-1,1-Difluoroethylene and Its Complex with the Argon Atom. *J. Mol. Spectrosc.* **2014**, *305*, 25−33.

(22) Kisiel, Z.; Pszczółkowski, L.; Medvedev, I. R.; Winnewisser, M.; De Lucia, F. C.; Herbst, E. Rotational Spectrum of *Trans*−*Trans* Diethyl Ether in the Ground and Three Excited Vibrational States. *J. Mol. Spectrosc.* **2005**, *233*, 231−243.

(23) Watson, J. K. G., Aspects of Quartic and Sextic Centrifugal Effects on Rotational Energy Levels. In *Vibrational Spectra and Structure*, Durig, J. R., Ed.; Elsevier Scientific Publishing: Amsterdam, 1977; *6*, 1−89.

(24) Watson, J. K. G. Determination of Centrifugal Distortion Coefficients of Asymmetric-Top Molecules. *J. Chem. Phys.* **1967**, *46*, 1935−1949.

(25) van Eijck, B. P. Reformulation of Quartic Centrifugal Distortion Hamiltonian. *J. Mol. Spectrosc.* **1974**, *53*, 246−249.

(26) Pickett, H. M. The Fitting and Prediction of Vibration-Rotation Spectra with Spin Interactions. *J. Mol. Spectrosc.* **1991**, *148*, 371−377.

(27) Su, Z.; Borho, N.; Xu, Y. Chiral Self-Recognition: Direct Spectroscopic Detection of the Homochiral and Heterochiral Dimers of Propylene Oxide in the Gas Phase. *J. Am. Chem. Soc.* **2006**, *128*, 17126−17131.

(28) Jeziorski, B.; Moszynski, R.; Szalewicz, K. Perturbation Theory Approach to Intermolecular Potential Energy Surfaces of Van Der Waals Complexes. *Chem. Rev.* **1994**, *94*, 1887−1930.

(29) Parrish, R. M.; Burns, L. A.; Smith, D. G. A.; Simmonett, A. C.; De Prince, A. E., III; Hohenstein, E. G.; Bozkaya, U.; Sokolov, A. Y.; Di Remigio, R.; Richard, R. M.; et al. Psi4 1.1: An Open-Source Electronic Structure Program Emphasizing Automation, Advanced Libraries, and Interoperability. *J. Chem. Theory Comput.* **2017**, *13*, 3185−3197.